Microstructural Characterization of *Bombyx mori* Silk Fibers

Yu Shen, Michael A. Johnson, and David C. Martin*

Department of Materials Science and Engineering, Macromolecular Science and Engineering Center, 2022 H. H. Dow, University of Michigan, Ann Arbor, Michigan 48109-2136

Received February 24, 1998; Revised Manuscript Received July 27, 1998

ABSTRACT: The microstructure of *Bombyx mori* silk fibers before and after degumming was examined by transmission electron microscopy (TEM), selected area electron diffraction (SAED), wide-angle X-ray scattering (WAXS), and low-voltage high-resolution scanning electron microscopy (LVHRSEM). LVHRSEM micrographs of the neat cocoon revealed a network of pairs of twisting filaments. After degumming, there were only individual filaments showing a surface texture consistent with an oriented fibrillar structure in the fiber interior. WAXS patterns confirmed the oriented β-sheet crystal structure common to silkworm and spider (dragline) silks. Low-dose SAED results were consistent with the WAXS data and revealed that the crystallographic texture did not vary significantly across the fiber diameter. TEM observations of individual microtomed fibers indicated a nominally triangular cross section and a 0.5−2 μm sericin coating. After degumming to remove the sericin, a banded feature was revealed with a characteristic spacing of nominally 600 nm along the fiber axis. These bands were oriented in a roughly parabolic or V-shape pointing along one axis within a given fiber. We hypothesize that this orientation was induced by the extrusion and drawing during the spinning process. Equatorial dark field (DF) images revealed that axial and lateral sizes of the β-sheet crystallites in silk fibroin ranged from 20 to 170 nm and from 1 to 24 nm, respectively. Crazes developed in the degummed silk fiber parallel to the fiber direction. The formation of these crazes suggests that there are significant lateral interactions between microfibrils in silk fibers.

Introduction

Natural silk fibers have excellent mechanical properties. For example, domesticated (*Bombyx mori*) silk worm fibers possess a tensile modulus on the order of 5 GPa,[1] strengths of 400 MPa, and tensile elongations of 15% or more and are able to undergo quite large deformations in compression without kinking. The mechanical performance of silk is even more remarkable since the fibers are produced under ambient conditions from aqueous solutions. *B. mori* silk fibers consist primarily of two components, fibroin and sericin; fibroin is the structural protein of the silk fiber, and sericin is the water-soluble glue that serves to bond fibers together. The majority of the fibroin is highly periodic with simple repeating sections broken by more complex regions containing amino acids with bulkier side chains.[2] The basic, highly repetitive sections are composed of glycine (45%), alanine (30%), and serine (12%) in a roughly 3:2:1 ratio.[2−4] These three residues contain short side chains and permit close packing of crystals through the stacking of hydrogen-bonded β-sheets. The structure is dominated by $[Gly\text{-}Ala\text{-}Gly\text{-}Ala\text{-}Gly\text{-}Ser]_n$ sequences, with corresponding side groups of H, CH_3, H, CH_3, H, CH_2OH. The sericin proteins, which comprise approximately 25 wt % of the silkworm cocoon, contain glycine, serine, and aspartic acid totaling over 60%. Compositional details for the silks can be found in a number of references.[2−4]

Warwicker[5] compared the X-ray patterns from over 70 different silks produced by species in the classes Insecta and Arachnida. When indexed using the molecular model for extended polypeptides of Marsh, Corey, and Pauling,[6] the groups showed the same basic crystalline structure. The chain axis and hydrogen bonding dimensions were similar for all silks, while differences arose in the intersheet spacing. These variations could be attributed to the different amino acid compositions and sequences of the fibroins. The unit cell dimensions were 0.695 nm along the fiber axis (*c*) and 0.944 nm for the interchain spacing (*a*). The intersheet spacing (*b*) varied from 0.93 to 1.57 nm.

Previous studies of the crystallinity in *B. mori* silk have revealed two different structural models, termed Silk I and Silk II.[3,5,7−9] Silk II is understood to be the extended β-sheet conformation as described previously. Silk I can be obtained by quiescent drying of the contents of the silk gland. The Silk II polymorph is more stable than the Silk I phase; attempts to induce orientation of the polymer chains for X-ray or electron diffraction studies tend to cause the Silk I to convert to Silk II. If the contents of the gland are spun, or mechanically sheared or rolled, Silk II is obtained. Conversion back to Silk I is accomplished by dissolving the fibroin in a solvent such as aqueous lithium bromide and successive dialyzation against water. Because of the irreversible phase change during the spinning process, natural silk fibers spun from aqueous solution are water insoluble.

The β-sheet crystallites have been detected by wide-angle X-ray scattering[5,6,8−11] of both spider dragline and silkworm cocoon silks. The NMR data from Nicholson et al.[12] and Asakura et al.[13] have refined the Silk II structure originally described by Marsh, Corey, and Pauling.[6] A high degree of orientation is seen in most fibers studied.[5] Cunniff et al.[11] and Mahoney et al.[14] reported morphological aspects of the dragline silk of *Nephila clavipes* by using LVHRSEM and AFM. Through examination of knots in the spider dragline silk, the compressive side of a given bend showed no kinking even with bend radii on the same order as the fiber

* To whom correspondence should be addressed. Telephone: (734) 936-3161. Fax: (734) 763-4788. E-mail: milty@umich.edu. WWW: http://www-personal.engin.umich.edu/∼milty.

10.1021/ma980281j CCC: $15.00
Published on Web 11/12/1998

diameter. This was attributed to the absence of a fibrillar structure. However, the fibrillar texture observed in abraded fibers indicates a modulation in properties consistent with the presence of microfibrils.

The processing steps to form fibers from the silk solution may be crucial to their mechanical performance. Evidence for a liquid crystalline phase in the precursor solution has been presented.[7,15] The transition from the liquid crystal to solid state has recently been probed through structural characterization by solution and solid-state NMR.[13,16] Solid state ^{2}H NMR and WAXS by Jelinski's group[17,18] on spider dragline silk (*N. clavipes*) indicated that two distinct levels of orientation exist for the Silk II β-sheet structure. The less oriented regions may correspond to single layers of hydrogen bonded sheets formed during the initial stages of crystallization, perhaps even while the fibroin solution is still in the liquid crystalline state.

Thiel et al.[19] found a modulation in contrast along the axis of *N. clavipes* dragline fibers. This 200 nm mesoscopic spacing was attributed to compositional fluctuations, distinct from sectioning artifacts and thickness variations. This dimension was on the same order of magnitude for the cholesteric helix (250 nm) found in the gland by Willcox et al.[15] The complicated but consistent amino acid sequences in silk proteins may lead to structural features on the submicron length scale. It is also possible that the morphology at these dimensions may be related to the liquid crystallinity of protein solutions and the variations in order induced during processing.

Thiel et al.[19] estimated crystallite sizes in the range of 70−100 nm from TEM imaging and diffraction. However, the sharpness and symmetry of the observed electron diffraction spots were not shown to be consistent with the WAXS patterns from bulk fibers. Smaller estimates for the crystallites were obtained by synchrotron WAXS patterns obtained by Grubb and Jelinski.[18] Minimum dimensions of 5 × 2 × 7 nm (intersheet, hydrogen bond and chain directions) were reported. These values were calculated by assuming a perfect crystal and fitting peaks with unmixed directions. The crystallites were highly oriented (15.7° of full width half-maximum), and the degree of crystallinity was estimated to be 10−15%.

Our purpose was to examine the microstructure of native and degummed *B. mori* silk fibers by using bright field (BF) and dark field (DF) TEM, SAED, WAXS, and LVHRSEM to obtain information about the dispersion of crystalline domains, size, shape, orientation, and crystal habit of the crystallites and the connectivity of silk crystallites. We also wanted to investigate the possibility of characterizing the silk fiber microstructure at the submicrometer length scale that is above that readily probed by X-ray diffraction but below that of the fiber diameter. This information is vital to fully understand how these factors influence the unusual physical properties of silk fibers. We compared our results with previous work done on both silkworm and spider silks. The mechanical properties of the silk fibers were also examined through lateral deformation studies. We anticipate that the results obtained in this work will be useful in the understanding the structural evolution during the spinning process and the rheological behavior of silk in the gland of the silkworm.

Experimental Section

TEM Specimen Preparation and Degumming. Narrow strips were cut from silk cocoons supplied by Marion Goldsmith at the Department of Zoology, University of Rhode Island. These were embedded in epoxy and cured at 60 °C for at least 48 h. Blocks were carefully trimmed for microtoming, which was performed using a Reichert-Jung UltraCut E ultramicrotome with a diamond knife. Cross sections and longitudinal through sections were produced. The longitudinal sections were cut on planes parallel to the fiber axis, with the knife direction intentionally chosen to be 20−30° from the fiber axis in order to distinguish sectioning artifacts, such as knife marks and chatter, from structural details. Sections were collected by retrieval from deionized water with 400 mesh copper grids. Sections were approximately 60 nm thick and were therefore suitable for TEM analysis after coating with a thin carbon layer. Certain specimens were decorated with gold as a reference for SAED experiments. TEM was performed using low-dose procedures on a 200 kV JEOL 2000 FX and a 400 kV JEOL 4000 EX. Kodak 4489 film was used on the 2000 FX and SO-163 on the 4000 EX.

The procedure of degumming *B. mori* cocoon fibers followed methods widely used in the textile industry.[3] Specimens were boiled in 1% aqueous sodium C14−16 olefin sulfonate/sodium lauryl sulfate surfactant solution for 45 min and then boiled in aqueous 0.5% soap solution for 30 min. The fibers were rinsed by sonication in deionized water for 10 min and allowed to dry in air for 2−3 days. TEM specimen preparation of degummed fibers was the same as the as-spun fibers.

Low-Voltage High-Resolution SEM. A Hitachi S-800 low voltage, high-resolution SEM with a field emission gun was used to examine the morphology of *B. mori* fibers. The strips from the cocoon or the bundles of degummed fibers were attached to the sample stub using conductive double stick tape and was coated with approximately 20 nm of Au−Pd alloy prior to being imaged at 2−5 kV.

WAXS. WAXS experiments were performed on a Rigaku fine-focus fixed tube generator with Ni-filtered Cu Kα radiation (λ = 0.154 nm), and a flat-film camera with pinhole collimation. Well-aligned fiber bundles of *B. mori* fibers both before (as-spun) and after degumming were mounted vertically at the exit of the collimator. Si and Ni powder standards were used for calibration. Typical camera lengths used were 1.8 or 3 cm.

Fourier Transforms and Optical Density Measurements. Quantitative analysis of images for Fourier transforms and optical density measurements were done with NIH Image 1.60. Images were scanned on a Leafscan 45 negative scanner with a resolution of 600 dpi. Optical density (OD) measurements were calibrated with Kodak optical density scale, no. 1A with a range of 0.05−3.05. Linearity in the intensity values for scanned negatives was verified by comparing to the known values of the optical density scale converted using

$$\mathrm{OD} = \log[I_o/I] \tag{1}$$

Results and Discussion

WAXS. The WAXS data of the fibers before and after degumming both included a 0.698 nm fiber period, which is a characteristic of the β-sheet crystal structure. In this structure, long segments of extended planar zigzag chains run parallel or antiparallel to neighboring chains, enabling a high density of hydrogen bonds to form between the carbonyl and amine groups. The coplanarity of the amide groups along the peptide backbone causes sheet formation when the chains hydrogen bond. These sheets readily packed together into crystals due to the small residues in the poly(GAGAGS) sequence.

Figure 1a shows a WAXS pattern of a bundle of cocoon fibers before degumming. The fiber axis is vertical. This

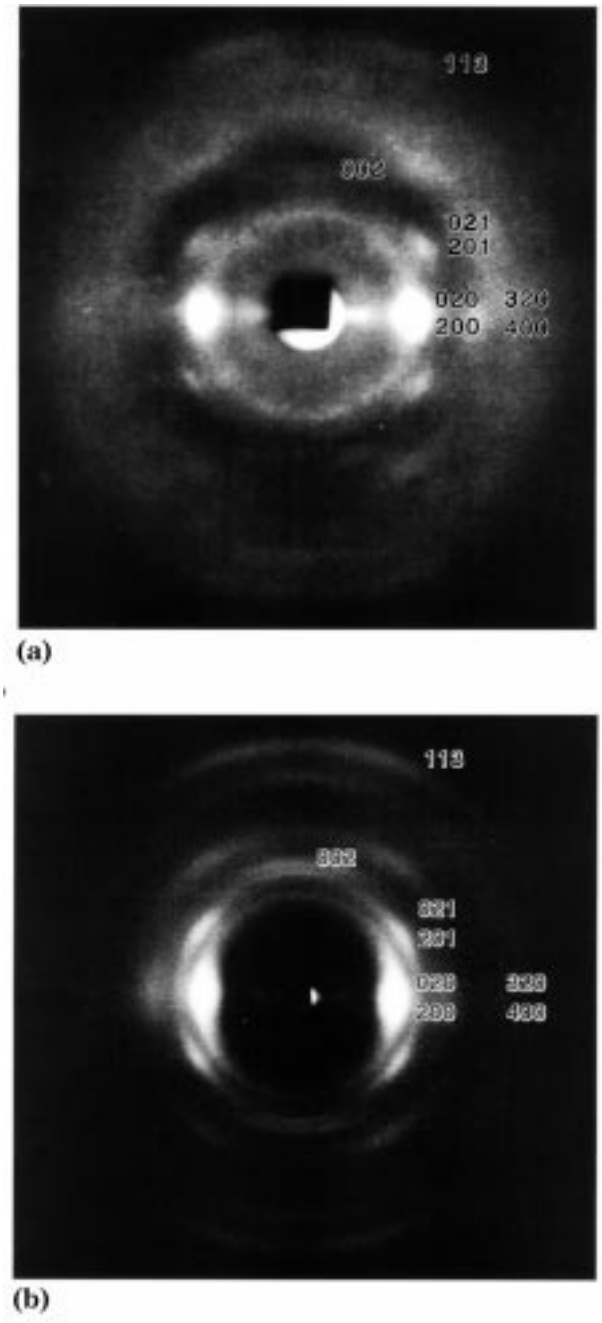

Figure 1. WAXS patterns of a bundle of cocoon fibers before (a) and after (b) degumming. Fiber axis is vertical.

pattern agreed with an oriented β-sheet structure in the crystallites of *B. mori* fibers. Various unit cell directions have been assigned: the hydrogen bonding and chain directions were placed in the $a-b$ plane by Marsh et al.,[6] the $b-c$ plane by Warwicker,[5] and in the $a-c$ plane by Takahashi.[9] This paper will follow Takahashi's assignment. The observed reflections could be indexed with a unit cell, $a = 0.944$ nm for the interchain direction, $b = 0.895$ nm for the intersheet distance, and $c = 0.700$ nm along the fiber axis (see Table 1).[20] Our analysis has not been able to distinguish between parallel and antiparallel packing of the β-sheet chains. Energetic analyses[9] and regular chain folding would favor antiparallel packing, but preferential orientation of the chains induced during spinning may drive the system to adopt parallel packing. This will be discussed in more detail later.

Table 1. Observed and Calculated *d*-Spacings of Silk II with a Unit Cell of $a = 0.944$ nm, $b = 0.895$ nm, and $c = 0.700$ nm

	obsd (nm)	calcd[21] (nm)	indices
d_1	0.895	0.896	(010)
d_2	0.448	0.448	(020)
d_3	0.370	0.377	(021)
$d_{4'}$	0.350	0.349	(002)
d_4	0.326	0.325	(012) or (220)
d_5	0.301	0.299	(030)
d_6	0.281	0.275 or 0.285	(022) or (130)
d_7	0.231	0.233	(003)
d_8	0.209	0.206 or 0.209	(023) or (420)
d_9	0.226	0.224	(040)

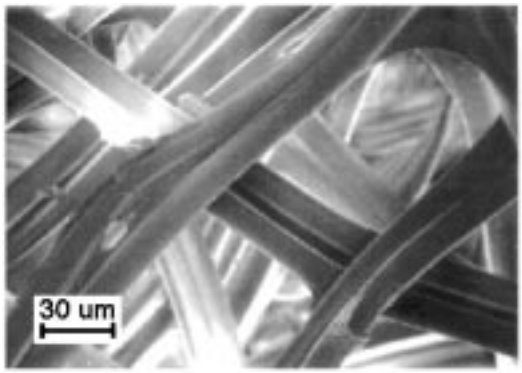

Figure 2. SEM micrograph of neat cocoon fibers before degumming with a network of pairs of twisting filaments.

Figure 1b is the corresponding WAXS patterns of the *B. mori* fibers after the degumming process. The basic features of the WAXS patterns of degummed fibers are identical to those of the fibers before degumming as well as in close agreement with other reported values of silk and poly(L-alanylglycine).[5,6,9,18,21]

Low-Voltage High-Resolution SEM. Figure 2 shows an SEM micrograph of cocoon fibers in a network of pairs of twisting filaments. Two fibers are spun simultaneously and are bonded to each other and to the cocoon by sericin. The fiber surfaces appeared smooth when viewed at low magnifications, and the diameter varied in the range 12−15 μm. However, after degumming, the fibers were cleanly separated into individual strands as shown in Figure 3a. The diameters were in the range of 10−13.7 μm, and therefore the sericin gum thicknesses could be estimated at 1−2 μm. Figure 3b shows a similar micrograph at higher magnification, showing the microfibrillar topography on the surface parallel to the fiber axis. Ridges persisted for microns while the fibril spacing was on the order of 100 to 200 nm.

TEM. Figure 4 shows a BF image by TEM of cross sections of *B. mori* fibers before the degumming process. The cross sections revealed shape and diameter variations in the fibers. The images also revealed a 0.5−2 μm coating of sericin around the fiber. The thickness of the coating was consistent with the estimate obtained from LVHRSEM (Figures 2 and 3). This shell−core morphology was also observed in longitudinal sections of the *B. mori* fiber. Figure 5 is an image of the longitudinal section of the cocoon fiber obtained from the defocused central spot of the SAED pattern to maximize contrast. The dark strip along the fiber edge corresponds to the sericin coating of the *B. mori* fiber.

To obtain information on crystallite size, orientation and arrangements, DF images of the cocoon fiber from

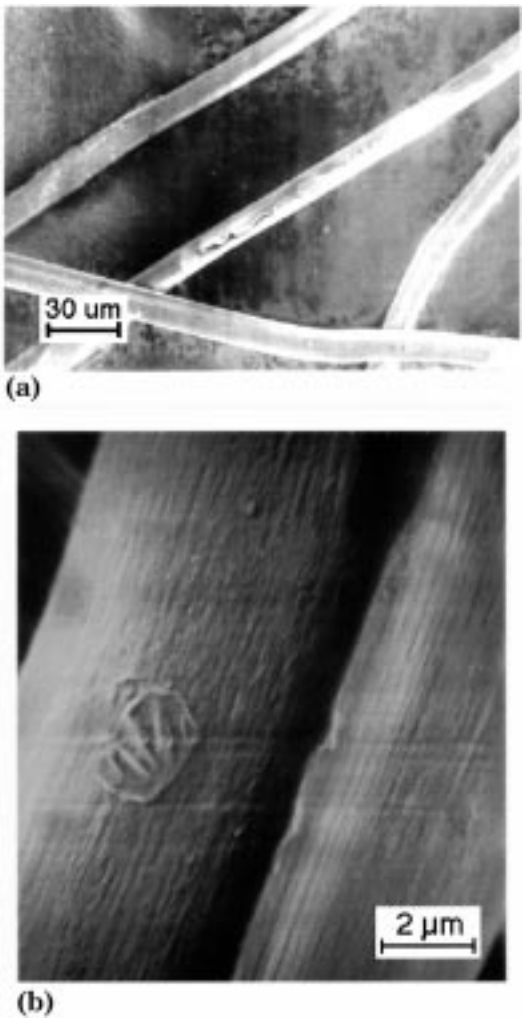

Figure 3. SEM micrographs of the cocoon fibers after degumming, revealing individual fibers (a) and microfibrillar structure (b) under high magnifications.

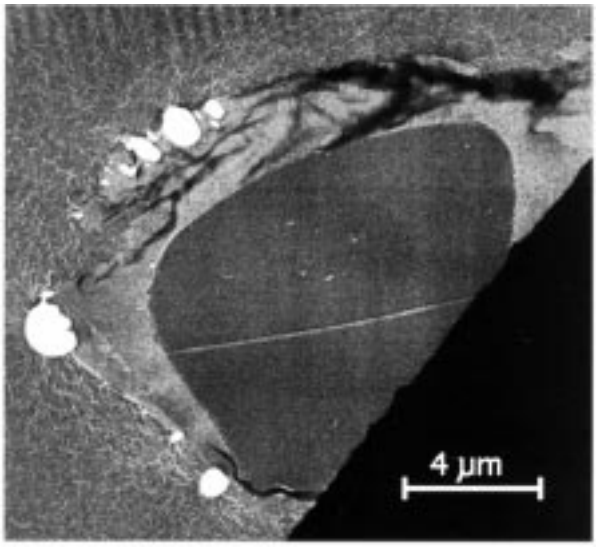

Figure 4. BF image of a cross section of a fiber before degumming.

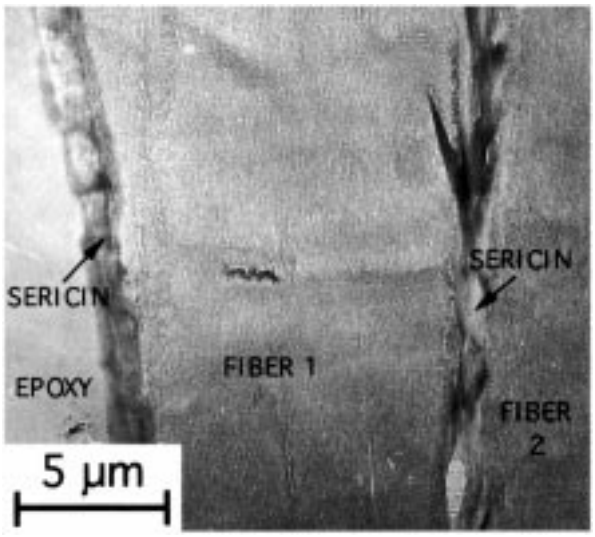

Figure 5. Defocused central spot of the ED pattern of a longitudinal section of fiber before degumming.

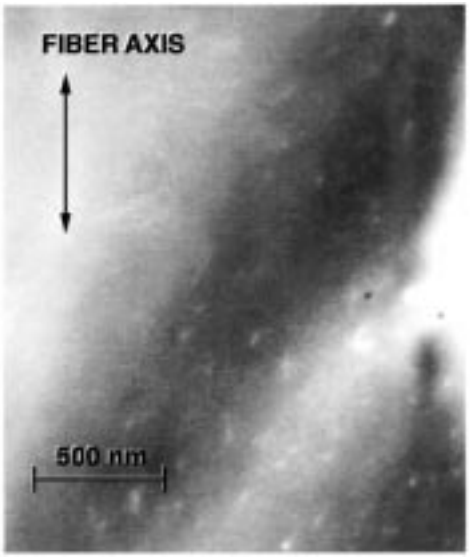

Figure 6. DF image of equatorial (020) reflections of a longitudinal section before degumming showing crystallites.

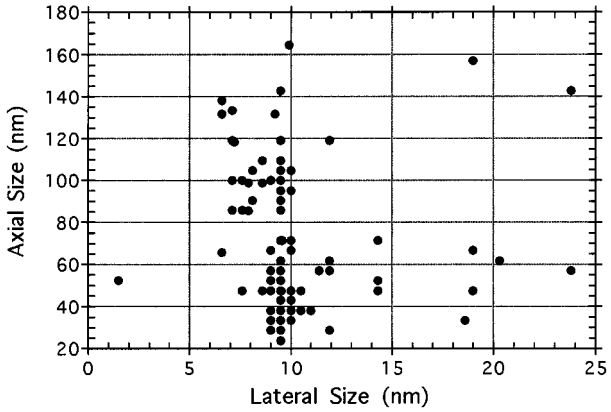

Figure 7. Plot of the lateral and axial size distributions of the β-sheet crystallites measured from the DF images.

the strongest (020) equatorial reflection before degumming were collected. Figure 6 is a DF image containing bright needlelike crystallites. The distributions of the axial and lateral sizes of the crystallites measured from the DF images are plotted in Figure 7. The crystallites were uniformly distributed in the whole fiber matrix with the molecular chains oriented essentially parallel to the fiber axis. The crystallites had a somewhat elongated shape with the long axis also parallel to the fiber axis. Quantitative examination of the images

revealed that the crystallites had lateral sizes of 10 ± 3 nm and axial sizes of 66 ± 34 nm. The axial dimension compared with Minoura's "crystalline" sequence length of approximately 350 nm, calculated using the β-sheet dimensions.[2] The SAED patterns confirmed that the molecular orientation was parallel to fiber axis direction regardless of the orientation of the crystallites themselves. The breadth of the diffraction spots corresponded to the small size of the crystallites. These observations were different from that of *N. clavipes* reported by Thiel et al.[19] In that report, the diffraction spots were quite sharp despite the distorted condition of the crystallites.

Figure 8a shows a low-dose SAED pattern of a degummed fiber microtomed along the fiber axis direction. A schematic of the SAED pattern with major reflections indexed is shown in Figure 8b. The SAED pattern was similar to the WAXS of degummed fibers. The low-dose SAED pattern confirmed the typical β-sheet crystal structure of *B. mori* fiber. The observed reflections of low-dose SAED of the longitudinal through section of degummed fiber were all consistent with WAXS data and were indexed using an orthorhombic unit cell with parameters, $a = 0.944$ nm (interchain distance in H-bond direction), $b = 0.896$ nm (intersheet distance) and $c = 0.698$ nm (fiber axis). The crystallographic texture was independent of the location across the fiber diameter. The uniformity of the electron diffraction across the fiber diameter indicated that there were no significant differences in crystallite size, orientation, and distribution throughout the fiber matrix.

Figures 9−11 are TEM images of longitudinal sections degummed *B. mori* of silk fibers. A number of unique characteristics were worth noting in these images. In all cases, the degumming process revealed periodic bands of contrast which were visible across the entire longitudinal section of the fiber. They were oriented in a roughly parabolic or V-shape pointing along the axis of the fiber, as is clearly shown in parts a and b of Figure 10. The curved bands had a characteristic spacing of nominally 600 nm along the fiber axis. Not all bands continued entirely across the section; a small fraction of band dislocations are visible in the line tracing of Figure 10b. The depth of the arc was approximately the same size as the fiber diameter but has shown to be influenced by the interaction of the microtome knife.

Digital FFT patterns were used to analyze the microstructure in more detail and are shown in insets in Figures 9 and 11. The FFTs adopts a 4-fold pattern consistent with the two major angles of the parabola. Strictly periodic parabolas would have manifested themselves in parallel lines, whereas deviation from parallel indicated that spacings normal to the fiber axis were larger than the projected spacings at the edges of the fiber. This was consistent with the observation of extra bands at the edge of the section.

The band orientation (tangent direction) relative to fiber axis direction at different location across the fiber diameter in Figures 9 and 10a are plotted in parts a and b of Figure 12, respectively. Deviations from parabolic to V-shaped bands were indicated by the dramatic change in angle near the center of the fiber (x-axis range of 0.4−0.6 in the figure). The more diffuse pair of lobes on the equator of the image correspond to the microfibrillar texture of the fiber section similar to the SAXS observations of spider silk done by Mahoney and Eby.[21]

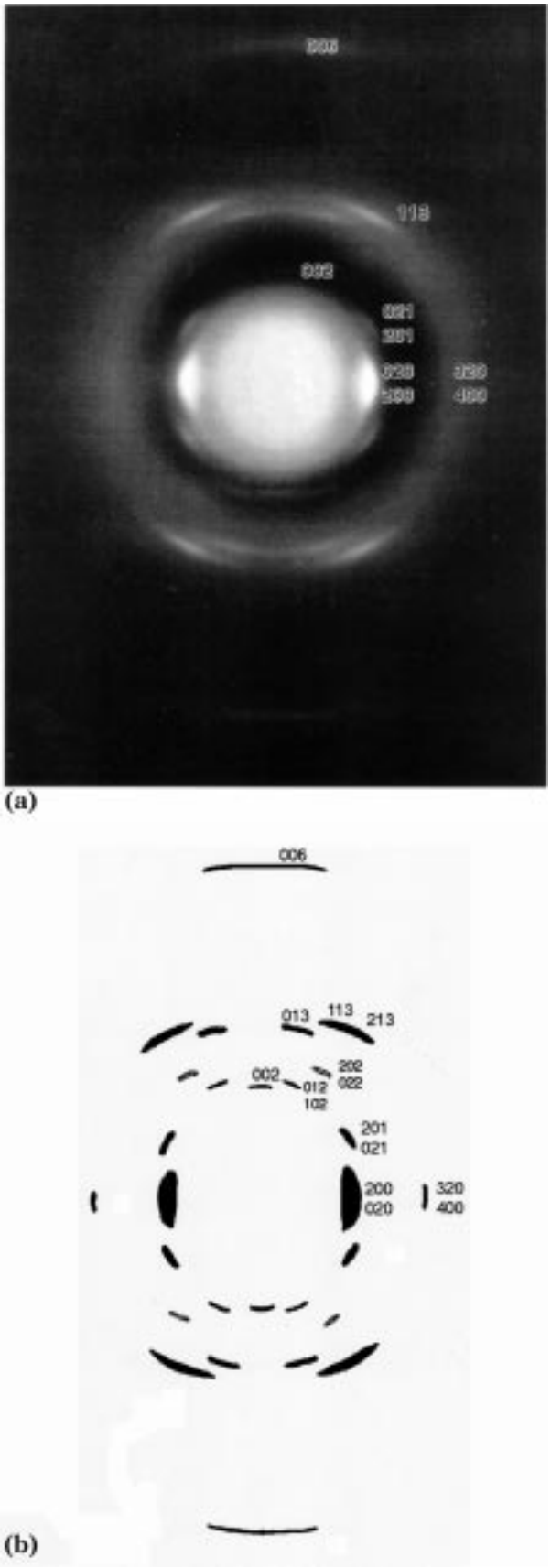

Figure 8. Low-dose SAED pattern of a degummed fiber microtomed through fiber axis direction (a) and a schematic representation of the SAED with indices of some important reflections (b).

The contrast in bright field TEM images corresponds to variations in mass-thickness of the sample. Ratios

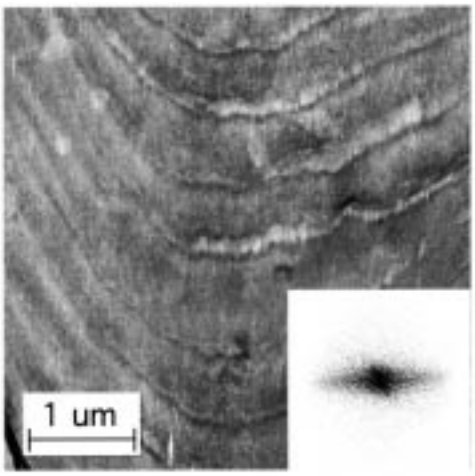

Figure 9. Defocused ED image of a longitudinal section of the degummed fiber with optical FFT inset.

of differences between regions were calculated using the relationship

$$I = I_O \exp[-S\rho t] \quad (2)$$

where S is the mass−thickness contrast parameter characteristic of the microscope and objective aperture, ρt was the mass-thickness value, and I_o was the incident intensity, derived from intensity values of holes in the specimen.[22] Calculations of the dark and light bands showed a mass-thickness difference of 50%. The average image density was 80% of the darkest areas, implying that the degumming process removed approximately half of the material in the lighter bands, with almost 20% removal overall. While the degumming process employed in this study used only a soap solution, the values for solubility compared with those compiled by Lucas[23] for fibroin separation by copper ethylenediamine, in which two fractions were isolated. The soluble fraction ranges from 10 to 50% of the fibroin depending on the method used for the separation.

A liquid crystalline intermediate phase of the aqueous silk solution may have a high degree of precrystalline molecular orientation.[17] Recently, Willcox et al.[15] presented evidence for a cholesteric liquid phase in the natural silk spinning process, for both *N. clavipes* and *B. mori*, through TEM and atomic force microscopy (AFM). In thin sections taken along the cryogenically quenched gland, they found periodicities of 250 nm in the spider gland and 600 nm in the silkworm gland. It was suggested that the spinning conditions could untwist the cholesteric helix and transform into a nematic phase and thus align the molecular chains with the flow direction. However, the helical axis was thought to run perpendicular to the flow direction of silk solution in the gland confounding a direct correlation between helix pitch and band spacing.

Because of the expected immiscibility of the sericin and fibroin, we hypothesize that the origin of the observed banding is due to a modulation of the fibroin itself. The two fractions of fibroin have drastic molecular mass differences, 350 and 25 kDa.[23] Molecular weight differences are evidently enough to cause segregation.[24] With this segregation into parabolic bands, the more soluble fraction may be etched away by the degumming process to reveal them as density contrast. The chain ends of the 350 kDa fraction, and possibly

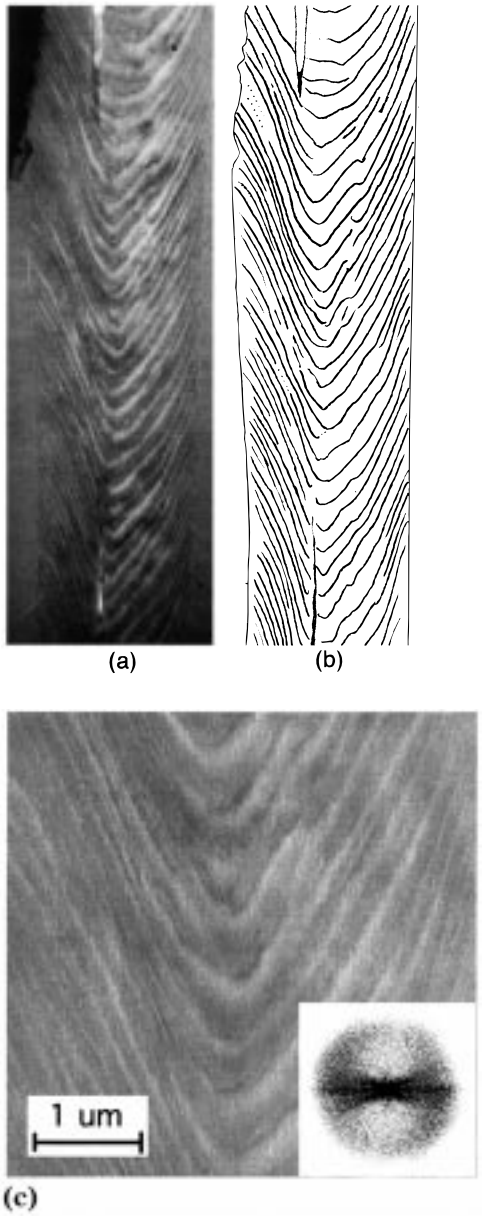

Figure 10. BF image (a), line tracing (b), and detail (c) of a longitudinal section of a degummed fiber.

chain folds, might also segregate to these regions. If this were the case, this region would contain sections with bulkier residues. The crystallinity would be lower, and the region would be more compliant.

The combination of the compliant banded regions and the roughly parabolic geometry may play an important role in determining the mechanical properties. The parabolic banding may allow for a distribution of stresses that would account for the unique combination of high modulus and large elongation to break. A simple model of the *B. mori* silk fiber structure is a stack of stiff bowls bonded together with a more compliant material. The parabolic shape would deform at the center while stresses near the outer surface would be translated to shear and be relieved by radial contraction. The harder phase parabolas could "cup" instead of transferring all strain to the softer phase. A difference in material properties between bands, including the anisotropy due to orientation, would be necessary. This difference is consistent with the electron density contrast in the TEM images (Figures 9 and 10). Other

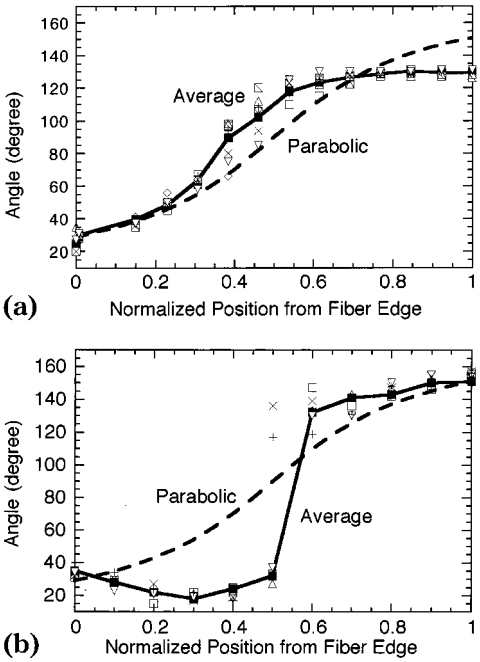

Figure 11. Plots of band orientation across the fiber section showing variation (a) and deviation (b) from parabolic geometry.

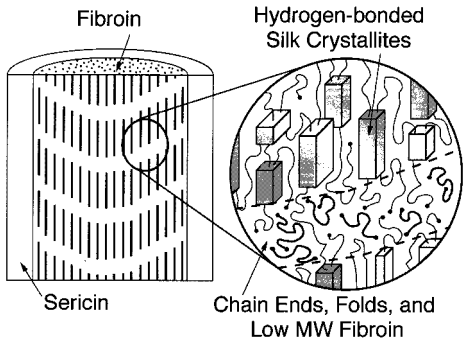

Figure 12. Model of microstructure of the *B. mori* silk fibroin.

models do not allow for this behavior. If compliant regions were randomly distributed throughout the fiber, the elongation would be limited by the harder phase. If the fiber were composed of flat lamella normal to the axis, the behavior would follow the softer phase. Work is being done on quantifying the contribution of geometry to the fiber properties through finite element analysis.

On the basis of the above evidence, we propose a model for the development of the microstructure of *B. mori* silk fibroin, represented schematically in Figure 12. In this model, the *B. mori* silk fibroin contains a crystalline-cross-linked network where the crystallites (dark rods) consist of stacked, antiparallel, hydrogen-bonding sheets. The large molecular weight fraction of molecules are nearly fully extended with their chain direction parallel to fiber axis. This oriented conformation may be established in the liquid crystalline phase in the gland and would require minimal reorientation as the fiber was drawn from the spinneret and dried. The reinforcing crystallites, which occupy up to 50−60% or more of the volume fraction of the fibroin, would lead to a high tensile strength and modulus in the degummed fiber. The molecular chains linking different crystallites remain coiled, flexible, and mobile and bridge between microfibrils to give lateral strength and allow elasticity

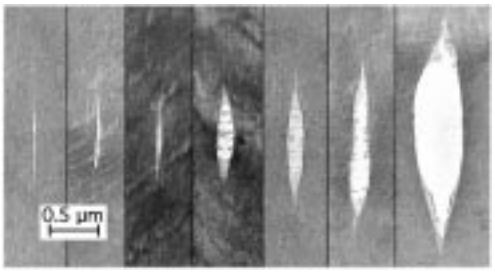

Figure 13. Compilation of crazes at different stages of development. Fiber axis is vertical.

through large deformations. The smaller molecular weight fraction would tend to segregate to areas with a higher density of chain ends, and would be removed by the degumming process.

An estimate for the larger (350 kDa) fibroin molecule is 5000 residues.[2] From the pleated β-sheet model,[5,6,9] there are 0.7-nm per dimer, which corresponds to a contour length of 1.8 μm. This is approximately three times the dimension of the band spacing, which implies at least some chain folding. Explicit chemical sequences and controlled processes have been proposed to allow positioning of hairpin turns in oriented polymers.[25,26] In the cocoon fibers of the silkworm, chain folds and bulky terminal ends may segregate to form the bands as well as forcing parallel packing which is energetically unfavorable. Flow of the liquid crystalline phase may align the crystallites into arrays that form the banded texture in the fiber. A simplified schematic of this model is shown in Figure 12.

Evidence for a microfibrillar substructure comes from both SEM and TEM experiments (Figures 3b and 5). Similar to the surface of the degummed fiber in Figure 3b, the contrast within the fiber section in Figure 5 indicates a microfibrillar structure. Close examination reveals periodicities parallel to the fiber axis. This periodicity is consistent with the SAXS data showing the presence of microfibrils.[21,27] The FFTs of the through sections also support the existence of these density fluctuations. This agrees with the LVHRSEM and the defocused ED images of the fibers. Water is dried from the silk cocoon fiber after it is drawn.[7] The sequence of extrusion, drawing, and finally evaporation evidently accounts for the generation of microfibrillar structures.

The crazes observed along the fiber axis in the degummed fiber indicate that reasonably strong lateral interactions existed between the fibrils. The fact that all the crazes ran parallel to fiber axis indicated that mechanical strength in the lateral direction of the fiber was weaker than that of the covalently bonded fiber direction. These filaments reached 100 nm before rupture, indicating that the interactions were strong enough to occasionally reorient polymer molecules. Figure 13 is a compilation of crazes imaged at different extents of deformation. The volume fraction of a craze can be calculated by

$$V_f = 1 - \frac{\ln(\Phi_{CRAZE}/\Phi_{HOLE})}{\ln(\Phi_{FILM}/\Phi_{HOLE})} \qquad (3)$$

where V_f is the volume fraction, i.e., the craze thickness relative to the sample thickness, and the F's are the image intensity values for the craze, hole, and bulk

film.[28] The calculation gave a V_f of 70% ± 20, which indicated a substantial lateral interaction.

Conclusions

The microstructure of *B. mori* silk fibers before and after degumming was examined by TEM, SAED, WAXS, and LVHRSEM. LVHRSEM micrographs of the neat cocoon revealed a network of pairs of twisting filaments. After being degummed, the individual filaments showed a surface texture consistent with an oriented fibrillar structure in the fiber interior. WAXS patterns confirmed the oriented β-sheet crystal structure common to silkworm and spider silks. Low-dose SAED results were fully consistent with the WAXS data, and revealed that the crystallographic texture did not vary significantly across the fiber diameter. Equatorial DF images revealed that axial and lateral sizes of the β-sheet crystallites in silk fibroin ranged from 20 to 170 nm and from 1 to 24 nm, respectively. Crazes developed in the degummed silk fiber parallel to the fiber direction. The formation of these crazes suggests that there are significant lateral interactions between fibrils in silk fibers. TEM observations of longitudinal sections of the degummed *B. mori* fiber showed banded features with a nominal characteristic spacing of 600 nm along the fiber axis. These bands were oriented in a roughly parabolic or V-shape pointing along one axis within a given fiber. We hypothesize that this shape is induced by extrusion during the spinning process. As yet, the mechanism of parabola formation is unknown, but some hypotheses for its presence include a flow profile modified by wall slip or a retraction mechanism after drawing. Work is being done to examine the direction of the bands in relation to the extrusion direction, and to analyze the effects of these bands on mechanical properties using finite element simulations.

Acknowledgment. The authors would like to acknowledge useful interactions and discussions with Christopher J. Buchko. Support for this research was provided by the National Institute of Health (NIH-NINDS program) N01-NS-5-2322, the National Science Foundation (NYI award to D.C.M.), Grant DMR-9257569, the Whitaker Foundation, and Protein Polymers Technologies, Inc.

References and Notes

(1) Grayson, M., Ed. *Kirk-Othmer Encyclopedia of Chemical Technology*; 3rd ed.; J. Wiley and Sons: New York, 1982; Vol. 20.
(2) Minoura, N.; Aiba, S.-I.; Higuchi, M.; *Biochem. Biophys. Res. Commun.* **1995**, *208*, 511−516.
(3) Kaplan, D. L.; Lombardi, S. J.; Muller, W. S. Fossey, S. A.; in *Biomaterials: Novel Materials from Biological Sources;* Byrom, D., Ed.; Stockton: New York 1991; pp 1−53.
(4) Mita, K.; Ichimura, S.; James, T.; *J. Mol. Evol.* **1994**, *38*, 583−592.
(5) Warwicker, J. O. *J. Mol. Biol.* **1960**, *2*, 350−362.
(6) Marsh, R. E.; Corey, R. B.; Pauling, L. *Biochim. Biophys. Acta* **1955**, *16*, 1−34.
(7) Magoshi, J.; Magoshi, Y.; Nakamura, S. In *Silk Polymers-Materials Science and Biotechnology*; Kaplan D. L., Adams W. W., Farmer, B. L., Viney, C., Eds.; American Chemical Society: Washington, DC, 1994; pp 292−310.
(8) Colonna-Cesari, F.; Premilat, S. Lotz, B. *J. Mol. Biol.* **1975**, *95*, 71−82.
(9) Takahashi, Y. In ref 7, pp 168−175.
(10) Fraser, R. D. B.; MacRae, T. P.; Steward, F. H. C.; Suzuki, E. *J. Mol. Biol.* **1965**, *11*, 706−712.
(11) Cunniff, P. M.; Fossey, S. A.; Auerbach, M. A.; Song, J. W.; Kaplan, D. L.; Adams, W. W.; Eby, R. E.; Mahoney, D. V.; Vezie, D. L. *Polym. Adv. Technol.* **1994**, *5*, 401−410.
(12) Nicholson, L. K.; Asakura, T.; Demura, M.; Cross T. A. *Biopolymers* **1993**, *33*, 847−861.
(13) Asakura, T.; Demura, M.; Uyama, A.; Ogana, K.; Komatsu, K.; Nicholson, L. K.; Cross T. A. In ref 7, pp 148−154.
(14) Mahoney, D. V.; Vezie D. L.; Eby R. K.; Adams W. W. Kaplan D. L. In ref 7, pp 196−210.
(15) Willcox, P. J.; Gido, S. P.; Muller, W.; Kaplan, D. L. *Macromolecules* **1996**, *29*, 5106−5110.
(16) Simmons, A.; Ray E.; Jelinski, L. W. *Macromolecules* **1994**, *27*, 5235−5237.
(17) Simmons, A. H.; Michal, C. A.; Jelinski, L. W. *Science* **1996**, *271*, 84−87.
(18) Grubb, D. T.; Jelinski, L. W. *Macromolecules* **1997**, *30*, 2860−2867.
(19) Thiel, B. L.; Kunkel, D. D. Viney, C. *Biopolymers* **1994**, *34*, 1089−1097.
(20) Fossey, S. A.; Kaplan, D. L. In ref 7, pp 270−282.
(21) Mahoney, D. V.; Eby, R. K., *Proc. 9th Int. Conf. Deformation, Yield Fracture* **1994**, 13.1−13.4.
(22) Misell, D. L.; Burdett, I. D. J. *J. Microscopy* **1977**, *109*, 171−182.
(23) Lucas, F.; Shaw, J. T. B.; Smith, S. G. In *Advances in Protein Chemistry*; Anfinsen, C. B., Anson, M. L., Bailey, K., Edsall, J. T., Eds.; Academic Press: New York, 1958; Vol. XIII, pp 107−222.
(24) Coleman, M. M.; Serman, C. J.; Bhagwagar, D. E.; Painter, P. C. *Polym. Rev.* **1990**, *31*, 1187−1203.
(25) Williams, D. R. M.; Warner, M. *J. Phys. Fr.* **1990**, *51*, 317−339.
(26) Irwin, R. S. *Macromolecules* **1993**, *26*, 7125−7133.
(27) Grubb, D. T.; Jackrel, D.; Jelinski, L. W. *Polym. Prepr.* **1997**, *38*, 73−74.
(28) Kramer, E. J. In *Crazing in Polymers*; Kausch, H. H., Ed.; Springer-Verlag: Berlin, 1983; p 26.

MA980281J